A Symbolic Formulation for Analytical Compliance Analysis and Synthesis of Flexure Mechanisms

Hai-Jun Su[1]
Assistant Professor
e-mail: su.298@osu.edu

Hongliang Shi
e-mail: shi.347@osu.edu

Department of Mechanical and Aerospace Engineering,
The Ohio State University,
Columbus, OH 43210

JingJun Yu
e-mail: jjyu@buaa.edu.cn

Robotics Institute,
Beihang University,
Beijing 100083, P. R. China

This paper presents a symbolic formulation for analytical compliance analysis and synthesis of flexure mechanisms with serial, parallel, or hybrid topologies. Our approach is based on the screw theory that characterizes flexure deformations with motion twists and loadings with force wrenches. In this work, we first derive a symbolic formulation of the compliance and stiffness matrices for commonly used flexure elements, flexure joints, and simple chains. Elements of these matrices are all explicit functions of flexure parameters. To analyze a general flexure mechanism, we subdivide it into multiple structural modules, which we identify as serial, parallel, or hybrid chains. We then analyze each module with the known flexure structures in the library. At last, we use a bottom-up approach to obtain the compliance/stiffness matrix for the overall mechanism. This is done by taking appropriate coordinate transformation of twists and wrenches in space. Four practical examples are provided to demonstrate the approach. A numerical example is employed to compare analytical compliance models against a finite element model. The results show that the errors are sufficiently small (2%, compared with finite element (FE) model), if the range of motion is limited to linear deformations. This work provides a systematical approach for compliance analysis and synthesis of general flexure mechanisms. The symbolic formulation enables subsequent design tasks, such as compliance synthesis or sensitivity analysis. [DOI: 10.1115/1.4006441]

1 Introduction and Motivations

Flexure mechanisms [1] are formed by multiple (often identical) flexure pivots or simple chains that are designed to produce a defined motion upon application of an appropriate loading. They are widely used in various precision instruments and machines [2] from nanomanipulators [3], nanopositioners [4], and optical scanning mirrors [5] to scanning transmission X-ray microscopy [6].

One important step toward the control and design of flexure mechanisms is the compliance analysis or mapping; the goal of which is to determine the relationship between the deformation and the loading applied to the device. Dimentberg [7] applied the screw calculus [8] to study the statics and vibration of an elastic suspension system. Loncaric [9] applied Lie algebra to the stiffness and compliance analysis of robotic devices and showed that the stiffness and compliance matrices can be reduced to a normal form by a particular choice of the coordinate frame. Lipkin and Patterson [10–12] studied the structure of compliance matrices via eigenvalue decomposition. Selig and Ding [13,14] applied the screw theory [15,16] to the compliance analysis of static beams. In their work, a general loading is represented by a wrench, while a general deformation is represented by a motion screw. They derived the compliance matrix for a cantilever beam subject to an end loading, and showed that the result was consistent with the classical one by Mises [17].

Much work has been done to study the compliance analysis and synthesis of flexure mechanisms. Awtar et al. [18] derived compliance matrix for 2D beams for studying the characteristics of various beam-based flexures. Dai and Ding [19] studied the compliance analysis of a vibratory bowl feeder mechanism formed by three leaf-spring flexures. Patil et al. [20] presented an analytical approach based on the screw theory for analyzing parasitic errors of flexure mechanism. Pei et al. [21] studied the stiffness and compliance of cartwheel flexural hinges. Recently Awtar and Sen [22,23] proposed a generalized constraint model for compliance and stiffness analysis of 2D beam flexures. Her and Midha [24] defined a compliance number (or degrees-of-compliance) concept for type synthesis of compliant mechanisms. Later one, Midha et al. [25] applied this technique for the type synthesis of compliant constant-force mechanisms. Huang and Schimmels [26,27] studied the synthesis of a compliance matrix with simple springs connected in serial or in parallel. Kim et al. [28] proposed a building block approach for compliance synthesis for planar mechanisms. This is further extended by Krishnan et al. [29,30], who studied serial and parallel concatenation of building blocks.

On the other hand, FE analysis [31] based approaches are widely used in the structural mechanics field for analyzing static deformation of the structures. In these approaches, structures are first divided into finite number of elements, and stiffness matrices [32] are then constructed based on the connectivity of these elements. However, the resulted matrices typically have a very high dimension depending on the number of elements. Petri [33] applied linear beam theories to derive stiffness matrices of 3D flexure mechanisms, which are then utilized for compliance synthesis. All these methods are basically numerical. The intrinsic characteristics of the compliance of flexure mechanisms are not explicitly identified.

In this paper, we propose a screw theory based approach for compliance analysis and synthesis of general 3D flexure mechanisms. The connectivity of individual elements or building blocks is systematically characterized by coordination transformation of screws (twists and wrenches). Rather in a numerical form, the compliance and stiffness matrices are derived in a symbolic form. The benefits of these symbolic formulas are that the designers can easily recognize the geometric interpretation of each element in a compliance or stiffness matrix. This also greatly simplifies subsequent tasks, such as design synthesis or sensitivity analysis. Compared with FE methods, this approach is much more efficient.

[1]Corresponding author.

Contributed by the Mechanisms and Robotics Committee of ASME for publication in the Journal of Mechanical Design. Manuscript received August 18, 2011; final manuscript received March 6, 2012; published online April 24, 2012. Assoc. Editor: Ashitava Ghosal.

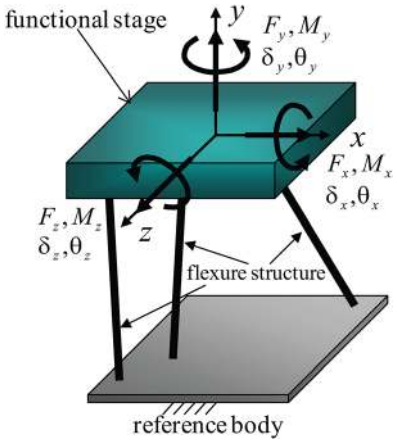

Fig. 1 A flexure mechanism is deformed by $\hat{T}$ under a general loading $\hat{W}$

The rest of the paper is organized as follows: Section 2 presents the definitions of compliance and stiffness as well as the problem statement. Section 3 derives the compliance and stiffness matrices for commonly used flexure elements. Section 4 studies compliance and stiffness matrices for flexure joints and simple chains, and in Sec. 5, we present basic steps for deriving the compliance and stiffness matrices of general flexure mechanisms. Also in this section, a compliant platform is employed to demonstrate the compliance analysis and synthesis process. The compliance matrix is verified by comparing with a finite element model. At last, Sec. 6 presents conclusions.

2 Compliance and Stiffness of Flexures

A general flexure mechanism is formed by connecting a functional stage to the base through one or more flexure elements, Fig. 1. The coordinate frame *oxyz* is placed at the stage, as we are interested in the motion of the stage. Let us denote the deformation by a general twist $\hat{T} = (\theta_x, \theta_y, \theta_z; \delta_x, \delta_y, \delta_z)$ with coordinates written in the frame *oxyz*, and the loading on the stage is denoted by a wrench $\hat{W} = (F_x, F_y, F_z; M_x, M_y, M_z)$. Both are column vectors. Our goal is to determine the mapping from $\hat{W}$ to $\hat{T}$ in terms of geometric and material parameters of the mechanism. In this paper, we assume that the deformation is sufficiently small so that the principle of linear elastic theory applies.

According to the elastic theory, the deformation twist and the loading wrench are related by

$$\hat{T} = [C]\hat{W}, \quad \hat{W} = [K]\hat{T}, \quad [C] = [K]^{-1} \tag{1}$$

where $[C]$ and $[K]$ are called 6×6 compliance and stiffness matrices, respectively.

2.1 Coordinate Transformation of Stiffness and Compliance Matrix. Let $\hat{T}$ and $\hat{W}$ be the twist and wrench represented in the coordinate frame $\mathcal{F}$. Very often, we have to describe a twist or a wrench in another coordinate frame $\mathcal{F}'$. To do so, we have to apply a coordinate transformation to twists, wrenches, or compliance/stiffness matrices. Suppose the coordinate transformation is represented by a 4×4 homogeneous matrix $[R,\mathbf{d}]$ with $[R]$ being the 3×3 rotation matrix and vector $\mathbf{d}$ being the translational part. The coordinates of a twist and a wrench in $\mathcal{F}'$ are calculated as

$$\hat{T}' = [Ad]\hat{T}, \quad \hat{W}' = [Ad]\hat{W} \tag{2}$$

where $[Ad]$ is the so-called 6×6 adjoint transformation matrix

$$[Ad] = \begin{bmatrix} R & 0 \\ DR & R \end{bmatrix} \tag{3}$$

Here, $[D]$ is the skew-symmetric matrix defined by the translational vector $\mathbf{d}$. The inverse of the adjoint transformation matrix is

$$[Ad]^{-1} = \begin{bmatrix} R^T & 0 \\ -R^T D & R^T \end{bmatrix} \tag{4}$$

where the superscript "T" represents the matrix transpose. These can be found in a number of graduate texts including Refs. [34] and [35].

The compliance matrix $[C']$ in the new coordinate system $\mathcal{F}'$ can be obtained as follows:

$$\hat{T}' = [Ad]\hat{T} = [Ad]([C]\hat{W}) = [Ad][C][Ad]^{-1}\hat{W}' \tag{5}$$

Similarly, we can obtain the new stiffness matrix $[K']$ in $\mathcal{F}'$. They are summarized below

$$[C'] = [Ad][C][Ad]^{-1}, \quad [K'] = [Ad][K][Ad]^{-1} \tag{6}$$

2.2 Compliance Analysis and Synthesis. Let $c_{ij}(\mathbf{p})$ and $k_{ij}(\mathbf{p})$ be the row i and column j elements of $[C]$ and $[K]$, respectively. Obviously, they are functions of the design parameters $\mathbf{p}$ that includes material properties, such as Young' modulus, geometric parameters of flexure elements, and the parameters related to assembly of flexure elements. Elements c_{ij} and k_{ij} represent the quantitative compliance or stiffness of the stage in the direction indicted by the index i caused by the loading indicated by the index j. For instance, c_{23} represents how much the stage rotates about the y axis due to a force along z axis, i.e., $c_{23} = \theta_y/F_z$.

In this paper, we study two problems: compliance analysis and compliance synthesis. The goal of the former is to derive $[C]$ with the mechanism parameters $\mathbf{p}$ given, and the goal of the latter is to find parameters $\mathbf{p}$ to achieve a desired compliance of the stage in the direction of interest. For instance, we would like to synthesize the stiffness of a linear spring formed by two parallel flexures. Assume the spring deforms in the x direction. We would chose the appropriate values for the design parameters $\mathbf{p}$ to achieve a prescribed value for compliance element $c_{41} = \delta_x/F_x$.

3 Commonly Used Flexure Elements

In this section, we seek to build a library of the compliance and stiffness matrices for various commonly used flexures.

3.1 Blade Flexures. Let us start with the most commonly used flexure element, a blade or sheet flexure. Figure 2 shows a blade flexure of length l, thickness t, and width w with $t \ll l$ and $t \ll w$. The compliance matrix of a blade flexure with a uniform

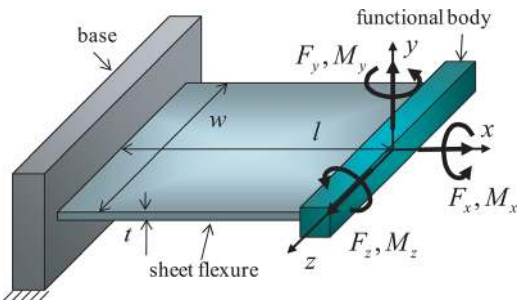

Fig. 2 A typical blade flexure with a rectangular cross section. The thickness is much smaller than the length, i.e., $t \ll l$.

cross section can be obtained by following the classical beam theory, such as Bernoulli–Euler beams. More specifically, the compliance matrix about the flexure center can be written as

$$[C_b^c] = \begin{bmatrix} 0 & 0 & 0 & \frac{l}{GJ} & 0 & 0 \\ 0 & 0 & 0 & 0 & \frac{l}{EI_y} & 0 \\ 0 & 0 & 0 & 0 & 0 & \frac{l}{EI_z} \\ \frac{l}{EA} & 0 & 0 & 0 & 0 & 0 \\ 0 & \frac{l^3}{12EI_z} & 0 & 0 & 0 & 0 \\ 0 & 0 & \frac{l^3}{12EI_y} & 0 & 0 & 0 \end{bmatrix} \tag{7}$$

where $A = tw$ is the area of the cross section, $I_y = tw^3/12$, $I_z = t^3w/12$ are the area moments, E,G are the Young's and shear modulus, and J is the torsion constant.

Note that in this paper, a wrench $\hat{W}$ is defined with the force vector preceding the moment vector, which is opposite to that found in Ref. [13]. If we swap the top three rows with the bottom three rows of $[C_b^c]$, we obtain a diagonal matrix previously obtained by Selig [13].

Very often, it is more convenient to derive the compliance matrix at the free end of the flexure. This can be easily done by applying a pure translation along x direction for $-l/2$ to $[C_b^c]$. The corresponding adjoint transformation matrix is written as

$$[Ad] = \begin{bmatrix} I & 0 \\ D & I \end{bmatrix}, \quad [D] = \begin{bmatrix} 0 & 0 & 0 \\ 0 & 0 & \frac{l}{2} \\ 0 & -\frac{l}{2} & 0 \end{bmatrix} \tag{8}$$

Substituting Eqs. (7) and (8) into Eq. (6) yields the compliance matrix written in the coordinate system at the end of the blade

$$[C_b] = [Ad][C_b^c][Ad]^{-1} = \begin{bmatrix} 0 & 0 & 0 & \frac{l}{GJ} & 0 & 0 \\ 0 & 0 & -\frac{l^2}{2EI_y} & 0 & \frac{l}{EI_y} & 0 \\ 0 & \frac{l^2}{2EI_z} & 0 & 0 & 0 & \frac{l}{EI_z} \\ \frac{l}{EA} & 0 & 0 & 0 & 0 & 0 \\ 0 & \frac{l^3}{3EI_z} & 0 & 0 & 0 & \frac{l^2}{2EI_z} \\ 0 & 0 & \frac{l^3}{3EI_y} & 0 & -\frac{l^2}{2EI_y} & 0 \end{bmatrix} \tag{9}$$

It can be seen that $[C_b]$ is determined by five independent design parameters $\mathbf{p} = (E,G,t,w,l)$.

For convenience, we normalize Eq. (9) to obtain

$$[C_b] = \frac{l}{EI_z} \begin{bmatrix} 0 & 0 & 0 & \frac{1}{\chi\beta} & 0 & 0 \\ 0 & 0 & -\frac{l\kappa}{2} & 0 & \kappa & 0 \\ 0 & \frac{l}{2} & 0 & 0 & 0 & 1 \\ \frac{l^2\eta}{12} & 0 & 0 & 0 & 0 & 0 \\ 0 & \frac{l^2}{3} & 0 & 0 & 0 & \frac{l}{2} \\ 0 & 0 & \frac{l^2\kappa}{3} & 0 & -\frac{l\kappa}{2} & 0 \end{bmatrix} \tag{10}$$

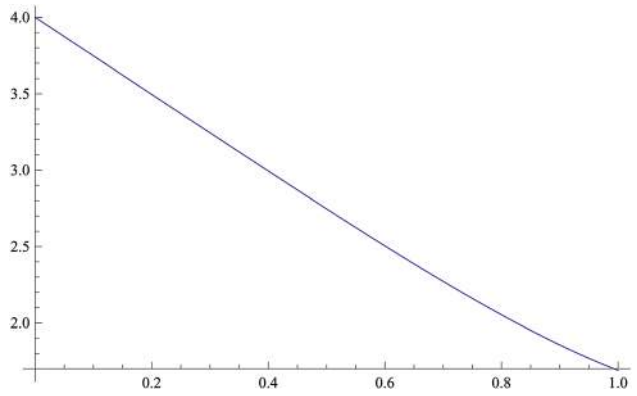

Fig. 3 The ratio β versus t/w

where

$$\kappa = \frac{I_z}{I_y} = \frac{t^2}{w^2}, \quad \beta = \frac{J}{I_z}, \quad \eta = \frac{t^2}{l^2}, \quad \chi = \frac{G}{E} = \frac{1}{2(1+\nu)} \tag{11}$$

are the nondimensional constants determined by geometries and material properties. ν is the Poisson's ratio. And β is the ratio of torsion constant over moment of inertia [36]. For a rectangular cross section, β is defined by

$$\beta = 12\left(\frac{1}{3} - 0.21\frac{t}{w}\left(1 - \frac{1}{12}\left(\frac{t}{w}\right)^4\right)\right) \tag{12}$$

which is plotted in Fig. 3. One can see that when t/w is sufficiently small, $\beta \approx 4$.

For a blade flexure, i.e., $\kappa \ll 1$ and $\eta \ll 1$, the compliance matrix $[C_b]$ depends on five new design parameters $\mathbf{p}_b = (l/EI_z,\chi,\kappa,\eta,l)$. It is not hard to see that the elements in the columns 1, 3, and 5 of $[C_b]$ are relatively small and can be neglected for the qualitative study. Furthermore, the location of the instant center can be readily obtained from columns 2, 4, and 6. See Su [37] for detailed qualitative study.

The stiffness matrix is the inverse of the compliance matrix calculated as

$$[K_b] = [C_b]^{-1} = \frac{EI_z}{l} \begin{bmatrix} 0 & 0 & 0 & \frac{12}{l^2\eta} & 0 & 0 \\ 0 & 0 & -\frac{6}{l} & 0 & \frac{12}{l^2} & 0 \\ 0 & \frac{6}{l\kappa} & 0 & 0 & 0 & \frac{12}{l^2\kappa} \\ \chi\beta & 0 & 0 & 0 & 0 & 0 \\ 0 & \frac{4}{\kappa} & 0 & 0 & 0 & \frac{6}{l\kappa} \\ 0 & 0 & 4 & 0 & -\frac{6}{l} & 0 \end{bmatrix} \tag{13}$$

3.2 Wire Flexures or Slender Rods. When both width and thickness are much smaller than the length, i.e., $t \ll l$ and $w \ll l$, the sheet flexure becomes a wire flexure. The compliance and stiffness matrices of a wire flexure have the same form as that of the blade flexures except that κ is not sufficiently small as the width w is comparable with the thickness t. If the cross section of a wire flexure is a circle of diameter $d \ll l$ (Fig. 4), the compliance matrix (10) can be simplified by substituting $A = \pi d^2/4$, $I_y = I_z = \pi d^4/64$, $J = 2I_z$, written as

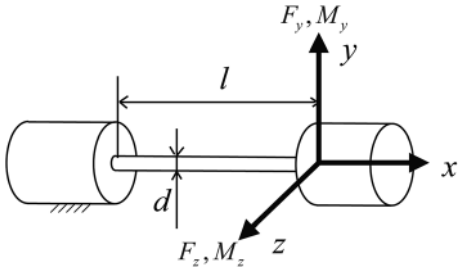

Fig. 4 A long wire flexure of diameter *d* and length *l* with $d \ll l$

$$[C_w] = \frac{l}{EI_z}\begin{bmatrix} 0 & 0 & 0 & \frac{1}{2\chi} & 0 & 0 \\ 0 & 0 & -\frac{l}{2} & 0 & 1 & 0 \\ 0 & \frac{l}{2} & 0 & 0 & 0 & 1 \\ \frac{l^2\eta}{16} & 0 & 0 & 0 & 0 & 0 \\ 0 & \frac{l^2}{3} & 0 & 0 & 0 & \frac{l}{2} \\ 0 & 0 & \frac{l^2}{3} & 0 & -\frac{l}{2} & 0 \end{bmatrix} \tag{14}$$

where $\eta = d^2/l^2$. It is not hard to see that the only nonzero element in first column $c_{41} = l^2\eta/16$ is sufficiently small and can be neglected. This leads that all elements in the first column are zeros. This further implies that the functional body does not deform under an axial loading. Physically, this agrees with our intuition that a wire flexure is very stiff along its longitudinal direction and very compliant in other directions [38].

And the stiffness matrix of a wire flexure is calculated as

$$[K_w] = [C_w]^{-1} = \frac{EI_z}{l}\begin{bmatrix} 0 & 0 & 0 & \frac{16}{l^2\eta} & 0 & 0 \\ 0 & 0 & -\frac{6}{l} & 0 & \frac{12}{l^2} & 0 \\ 0 & \frac{6}{l} & 0 & 0 & 0 & \frac{12}{l^2} \\ 2\chi & 0 & 0 & 0 & 0 & 0 \\ 0 & 4 & 0 & 0 & 0 & \frac{6}{l} \\ 0 & 0 & 4 & 0 & -\frac{6}{l} & 0 \end{bmatrix} \tag{15}$$

Clearly, the compliance or stiffness of a wire flexure with a circular cross section is determined by only four design parameters $\mathbf{p}_w = (l/EI_z, \chi, \eta, l)$.

3.3 Building a Library of Compliance Matrices. It is possible to repeat the above procedure for other kinds of flexure elements. Fortunately, there is an abundant work in the literature for calculating compliance of flexures with various geometries. For blade or wire flexures with a more complex cross section, we recommend using $[C_b]$ in Eq. (10). An alternative way is to find an equivalent circular cross section with the same area of moment inertia and area. For right circular notches, we can treat them as the short beam flexures. However, when a more accurate model is required, one can use the results in Ref. [39]. A more comprehensive receipt for single-axis and multiple-axis flexure hinges has been done by Lobontiu [40]. Recently Yong et al. [41] reviewed circular notch type flexure hinges. For helical springs, we would recommend using the compliance formulation derived by Ding and Selig [42]. Eventually, we can build a library of compliance matrices for commonly used flexure elements that can be used to construct flexure mechanisms with arbitrary topologies.

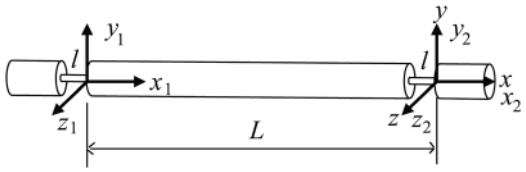

Fig. 5 A serial chain of two identical wires joined by a rigid rod of length *L*. Each wire has a length *l* and a diameter *d*.

4 Simple Flexure Chains

In this section, we study simple chains that are formed by two or more flexure elements. Depending on how the flexure elements are connected, we can have serial flexure chains or parallel flexure chains [25].

4.1 Serial Flexure Chains. A serial flexure mechanism is formed by connecting a functional body to a fixed reference body, through a serial chain of flexure elements that are joined with intermediate bodies. Let us denote the compliance matrix of the *j*th flexure element by $[C_j]$. The deformation of the functional body is the superimposition of the deformation of individual elements. However, all deformations must be written in the same coordinate frame before they can be summed. Mathematically, the overall compliance matrix of a serial flexure chain is calculated as

$$[C] = \sum_{j=1}^{m} [Ad_j][C_j][Ad_j]^{-1} \tag{16}$$

where $[Ad_j]$ is the coordinate transformation matrix from the *j*th flexure to the functional stage.

Example 1. Figure 5 shows a serial chain of two identical wire flexures that are separated by a rigid rod of length L along x axis. Assume both wires have a circular cross section of diameter d. If we place the coordinate system xyz coincides with the end of the second wire $x_2y_2z_2$, the coordinate transformations for these two wire flexures can be written as

$$[R_1] = [R_2] = [I], \quad \mathbf{d}_1 = (-L, 0, 0), \quad \mathbf{d}_2 = (0, 0, 0)$$

By following the formulation for serial chains, we obtain the compliance matrix for the serial chain as

$$[C_{ww}] = [Ad_1][C_w][Ad_1]^{-1} + [Ad_2][C_w][Ad_2]^{-1} =$$
$$\frac{l}{EI_z}\begin{bmatrix} 0 & 0 & 0 & \frac{1}{\chi} & 0 & 0 \\ 0 & 0 & -L-l & 0 & 2 & 0 \\ 0 & L+l & 0 & 0 & 0 & 2 \\ \frac{l^2\eta}{8} & 0 & 0 & 0 & 0 & 0 \\ 0 & L^2+lL+\frac{2l^2}{3} & 0 & 0 & 0 & L+l \\ 0 & 0 & L^2+lL+\frac{2l^2}{3} & 0 & -L-l & 0 \end{bmatrix} \tag{17}$$

$$\approx \frac{l}{EI_z}\begin{bmatrix} 0 & 0 & 0 & \frac{1}{\chi} & 0 & 0 \\ 0 & 0 & -L & 0 & 2 & 0 \\ 0 & L & 0 & 0 & 0 & 2 \\ \frac{l^2\eta}{8} & 0 & 0 & 0 & 0 & 0 \\ 0 & L^2 & 0 & 0 & 0 & L \\ 0 & 0 & L^2 & 0 & -L & 0 \end{bmatrix} \tag{18}$$

where the approximation step is based on the fact that $l \ll L$. If we would like to consider the second order of parasitic error, we

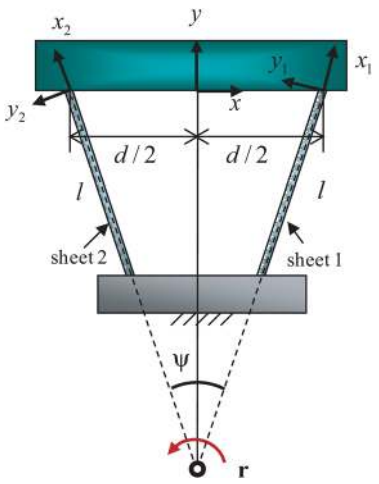

Fig. 6 A parallel flexure mechanism formed by two parallel ideal blade flexures

would use Eq. (17) for the following analysis. However, in this paper, we use Eq. (18) instead for the sake of simplicity. By taking a look at the second and the third column of $[C_{ww}]$ in Eq. (18), one can easily check that the instant rotation center for both F_y and F_z is actually the center of the first wire flexure. This agrees with our intuition.

To complete the analysis, we calculate the stiffness matrix of a serial chain of two wire flexures by inverting $[C_{ww}]$

$$[K_{ww}] = [C_{ww}]^{-1} = \frac{EI_z}{l}\begin{bmatrix} 0 & 0 & 0 & \frac{8}{l^2\eta} & 0 & 0 \\ 0 & 0 & -\frac{1}{L} & 0 & \frac{2}{L^2} & 0 \\ 0 & \frac{1}{L} & 0 & 0 & 0 & \frac{2}{L^2} \\ \chi & 0 & 0 & 0 & 0 & 0 \\ 0 & 1 & 0 & 0 & 0 & \frac{1}{L} \\ 0 & 0 & 1 & 0 & -\frac{1}{L} & 0 \end{bmatrix} \tag{19}$$

4.2 Parallel Flexure Chains. A parallel flexure mechanism is formed by connecting a functional body to a reference body through two or more flexure elements in parallel. Let us denote the stiffness matrix of the jth flexure element by $[K_j]$. For the same deformation of the stage, the force required will be the sum of the forces required for each element. As in serial flexure chains, all loads must be written in the same coordinate frame. Mathematically, the overall stiffness matrix of a parallel flexure chain is calculated as

$$[K] = \sum_{j=1}^{m} [Ad_j][K_j][Ad_j]^{-1} \tag{20}$$

where $[Ad_j]$ is the coordinate transformation operator from the jth flexure to the functional stage.

Example 2. Figure 6 shows a trapezoidal leaf-type flexure pivot that is formed by two identical blade flexures assembled symmetrically by an angle ψ at a distance d. We denote the length of the blade by l, width by w, and thickness by t. The coordinate transformations for blades 1 and 2 are, respectively

$$[R_1] = \left[Z\left(\frac{\pi-\psi}{2}\right)\right], \quad \mathbf{d}_1 = \left(\frac{d}{2}, 0, 0\right)$$

$$[R_2] = \left[Z\left(\frac{\pi+\psi}{2}\right)\right], \quad \mathbf{d}_2 = \left(-\frac{d}{2}, 0, 0\right)$$

Substituting the above transformation matrices and $[K_b]$ from Eq. (13) into Eq. (20) to obtain the following stiffness matrix:

$$[K_t] = [Ad_1][K_b][Ad_1]^{-1} + [Ad_2][K_b][Ad_2]^{-1} \tag{21}$$

And the compliance matrix is computed as

$$[C_t] = [K_t]^{-1} = \frac{l}{EI_z}\begin{bmatrix} 0 & 0 & c_{13} & c_{14} & 0 & 0 \\ 0 & 0 & 0 & 0 & c_{25} & 0 \\ c_{31} & 0 & 0 & 0 & 0 & c_{36} \\ c_{41} & 0 & 0 & 0 & 0 & c_{46} \\ 0 & c_{52} & 0 & 0 & 0 & 0 \\ 0 & 0 & c_{63} & c_{64} & 0 & 0 \end{bmatrix} \tag{22}$$

where c_{ij} are the nonzero compliance elements. See similar results in Refs. [43] and [44].

Let us take a look at the compliance of this flexure pivot subject to a moment loading M_z. That is, to consider the following two elements:

$$c_{36} = \frac{1}{2}\left[\frac{1+\eta+(\eta-1)\cos\psi}{6\rho^2+\eta+4+(\eta-4)\cos\psi-12\rho\sin\frac{\psi}{2}}\right] \tag{23}$$

$$c_{46} = \frac{l\cos\frac{\psi}{2}}{-2}\left[\frac{\eta+\rho(1-\eta)\sin\frac{\psi}{2}}{6\rho^2+\eta+4+(\eta-4)\cos\psi-12\rho\sin\frac{\psi}{2}}\right] \tag{24}$$

where $\rho = d/l$ and $\eta = t^2/l^2$. The element c_{36} represents the deformation θ_z due to the loading M_z, and c_{46} is the parasitic translational deformation δ_x.

To determine the position of the instant rotation center on the y axis, we compute

$$\frac{c_{46}}{c_{36}} = -l\cos\frac{\psi}{2}\left[\frac{\eta+\rho(1-\eta)\sin\frac{\psi}{2}}{1+\eta+(\eta-1)\cos\psi}\right] \tag{25}$$

It is intuitive to see that the nominal instant center is at the point $\mathbf{r} = (0, -d\cot\left(\frac{\psi}{2}\right)/2, 0)$ on the y axis, which is the intersection point of two flexures. (Fig. 6) The parasitic error of the instant center is calculated as

$$\Delta_{ry} = \frac{c_{46}}{c_{36}} + \frac{d\cot\left(\frac{\psi}{2}\right)}{2} = \frac{l\eta\cot\frac{\psi}{2}\left(\rho-\sin\frac{\psi}{2}\right)}{1+\eta+(\eta-1)\cos\psi} \tag{26}$$

The relative error Δ_{ry}/l is plotted in Fig. 7.

Figure 7 and Eq. (26) can be used in the synthesis of flexure joints. From Eq. (26), we can see that $\Delta_{ry} = 0$ if $\rho = \sin(\psi/2)$ which corresponds the case shown in Fig. 8(*a*). Designers can determine the geometric parameters η,ρ,ψ to minimize the error of instant center while meeting other design requirements.

Example 3. As a special case, when $\psi = 0$, we obtain the well known parallelogram linear spring as shown in Fig. 8(*b*). The rotational compliance of the parallelogram linear spring is obtained by substituting $\psi = 0$ into Eq. (23)

$$c'_{36} = \frac{1}{2}\left(\frac{\eta}{3\rho^2+\eta}\right) \tag{27}$$

To study the change of the compliance c_{36}, we plot the following ratio c_{36}'/c_{36} versus ψ with $\eta = 0.01$ and $\rho \in [0.5,4]$ (Fig. 9).

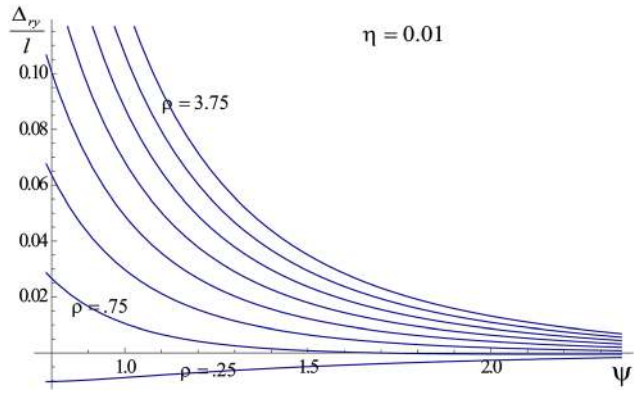

Fig. 7 The error of instant center Δ_{ry}/l versus $\psi \in [0,3\pi/4]$ with $\eta = 0.01$ and $\rho \in [0.25,3.75]$

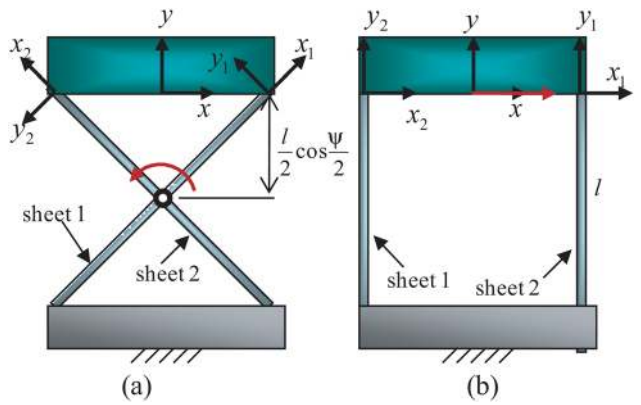

Fig. 8 (*a*) A typical cross-strip flexure pivot and (*b*) a parallelogram linear spring

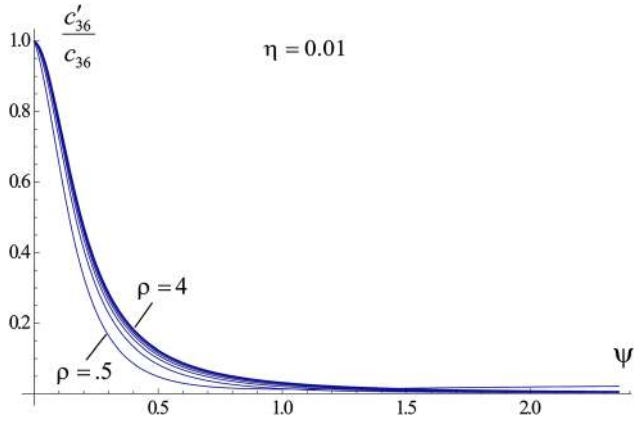

Fig. 9 The change of rational compliance versus $\psi \in [0,3\pi/4]$ with $\eta = 0.01$ and $\rho \in [0.5,4]$

We can see a drastic drop of this ratio as ψ approaches to $\pi/2$. In other words, the rotational stiffness of parallelogram is significantly larger than that of cross-strip flexure pivot when $\psi \geq \pi/2$.

Now, let us study the translational compliance along x axis and the parasitic error under a horizontal force. We consider the following two compliance elements:

$$\frac{\theta_z}{F_x} = c'_{31}\frac{l}{EI_z} = -\frac{l^2}{4EI_z}\left(\frac{\eta}{3\rho^2+\eta}\right) \tag{28}$$

$$\frac{\delta_x}{F_x} = c'_{41}\frac{l}{EI_z} = \frac{l^3}{24EI_z}\left(\frac{3\rho^2+4\eta}{3\rho^2+\eta}\right) \tag{29}$$

When η is sufficiently small, we have

$$\frac{\delta_x}{F_x} \approx \frac{l^3}{24EI_z}$$

which is 1/24 of the compliance of one blade flexure shown in Eq. (10). Obviously, δ_x/F_x gives the parasitic rotation caused by a lateral force F_x. As indicated in Eq. (28), when η is sufficiently small, this error is linearly proportional to η. The equivalent instant line of this parasitic rotation is a line parallel to z axis through a point on the y axis that is determined by the ratio of δ_x/F_x over θ_z/F_x. That is, dividing Eq. (29) by Eq. (28) yields

$$-r_y = \frac{l\rho^2}{2\eta} + \frac{2l}{3} \tag{30}$$

Equation (30) clearly shows that the separation distance $d = \rho l$ significantly shifts the instant center from $2l/3$ (one blade flexure) to a point far down the y axis as $\eta \ll \rho$. As a result, this flexure is considered equivalent to a linear spring.

5 General Flexure Mechanisms

Most practical flexure mechanisms are hybrid. Our compliance analysis and synthesis framework for general flexure mechanisms are based on the library of flexure elements built in Sec. 3 and the formulation for serial and parallel chains derived in Sec. 4.

The compliance analysis/synthesis for hybrid flexure mechanisms is described as follows. First, we subdivide the mechanism hierarchically into modules: serial/parallel chains until we reach the level of basic flexure elements previously studied in the library. Then, we apply the formulation derived in Sec. 4 to obtain the compliance and stiffness matrices for each of these modules, chains, and elements at their local coordinate system. We can use a bottom-up approach to build the compliance matrix for the entire flexure mechanism. In all steps, we try to keep all major geometric parameters in symbolic form whenever possible. This is possible with the help of modern computer algebraic software, such as MATHEMATICA or MAPLE. Ultimately, we aim to obtain a symbolic compliance matrix of the functional stage written in the task space.

For compliance analysis, we then substitute the numerical values for the geometric parameters into the compliance matrix. For compliance synthesis, we consider individual compliance elements, and chose a set of design parameters to achieve a desired compliance. In what follows, we use a spatial parallel compliant platform (Fig. 10) to demonstrate the process.

5.1 Derivation of the Compliance Matrix. The flexure mechanism is formed by three identical compliant limbs assembled symmetrically in parallel. To study the overall compliance of the platform, we use the following steps:

(1) Subdivide the compliant platform mechanism into three identical limbs. Each limb is a serial chain of two identical wire flexures notch hinges. The wire flexures have a length l and a circular cross section of diameter d.
(2) Derive the compliance matrix for each limb. This has already been done in Example 1 of Sec. 4.1. The compliance and stiffness matrices written in their local coordinate frame are given by $[C_{ww}]$ in Eq. (18) and $[K_{ww}]$ in Eq. (19), respectively.
(3) Derive the transformation matrix from the local coordinate system at each limb to the task space (coordinate frame on the stage). For limb 1, the coordinate transformation is obtained by the geometry shown in Fig. 10, written as

$$R_1 = \left[Z\left(\alpha+\frac{\pi}{2}\right)\right] = \begin{bmatrix} -\sin\alpha & -\cos\alpha & 0 \\ \cos\alpha & -\sin\alpha & 0 \\ 0 & 0 & 1 \end{bmatrix}, \quad \mathbf{d}_1 = \begin{bmatrix} r \\ -h \\ 0 \end{bmatrix} \tag{31}$$

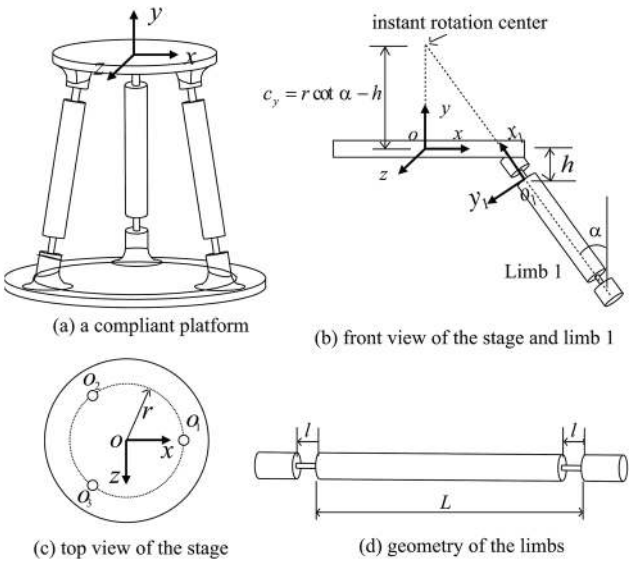

Fig. 10 A flexure platform mechanism with three identical chains of two wire flexures

And the transformations for limbs 2 and 3, $[R_2]$, $\mathbf{d}_2$, $[R_3]$, $\mathbf{d}_3$, are obtained by rotating the coordinate $o_1x_1y_1z_1$ about y axis for $2\pi/3$ and $-2\pi/3$, respectively. More specifically, they are written as

$$R_2 = \begin{bmatrix} \frac{\sin\alpha}{2} & \frac{\cos\alpha}{2} & \frac{\sqrt{3}}{2} \\ \cos\alpha & -\sin\alpha & 0 \\ \frac{1}{2}\sqrt{3}\sin\alpha & \frac{1}{2}\sqrt{3}\cos\alpha & -\frac{1}{2} \end{bmatrix}, \quad \mathbf{d}_2 = \begin{bmatrix} -\frac{r}{2} \\ -h \\ -\frac{\sqrt{3}r}{2} \end{bmatrix}$$

$$R_3 = \begin{bmatrix} \frac{\sin\alpha}{2} & \frac{\cos\alpha}{2} & -\frac{\sqrt{3}}{2} \\ \cos\alpha & -\sin\alpha & 0 \\ -\frac{1}{2}\sqrt{3}\sin\alpha & -\frac{1}{2}\sqrt{3}\cos\alpha & -\frac{1}{2} \end{bmatrix}, \quad \mathbf{d}_3 = \begin{bmatrix} -\frac{r}{2} \\ -h \\ \frac{\sqrt{3}r}{2} \end{bmatrix}$$

(4) Compute the adjoint transformation matrices for three limbs by substituting $R_i, \mathbf{d}_i (i = 1,2,3)$ into Eq. (3), i.e.

$$[Ad_j] = \begin{bmatrix} R_j & 0 \\ D_jR_j & R_j \end{bmatrix} \quad (j = 1,2,3) \tag{32}$$

(5) Substitute $[K_{ww}]$ from Eq. (19) and $[Ad_j]$ from Eq. (32) into Eq. (20) to obtain the stiffness matrix of the platform

$$[K_{3ww}] = \sum_{j=1}^{3} [Ad_j][K_{ww}][Ad_j]^{-1} \tag{33}$$

(6) Compute the compliance matrix of the platform by inverting the stiffness matrix $[K_{3ww}]$

$$[C_{3ww}] = [K_{3ww}]^{-1} = \frac{l}{EI_z} \begin{bmatrix} 0 & 0 & c_{13} & c_{14} & 0 & 0 \\ 0 & 0 & 0 & 0 & c_{25} & 0 \\ c_{31} & 0 & 0 & 0 & 0 & c_{36} \\ c_{41} & 0 & 0 & 0 & 0 & c_{46} \\ 0 & 0 & 0 & 0 & 0 & 0 \\ 0 & 0 & c_{63} & c_{64} & 0 & 0 \end{bmatrix} \tag{34}$$

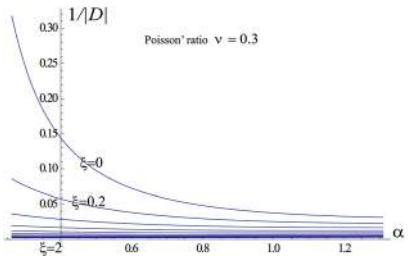

Fig. 11 The rotational compliance c_{25} versus $\alpha \in$ [15 deg,75 deg] with Poisson's ratio $\nu = 0.3$ and $\xi = r/L \in [0,2]$

where

$$c_{14} = c_{36} = \frac{16\sin^2\alpha}{|D|} \tag{35}$$

$$c_{31} = -c_{13} = c_{46} = -c_{64} = c_{14}c_y \tag{36}$$

$$c_{63} = c_{41} = c_{14}c_y^2 \tag{37}$$

$$c_{25} = \frac{8\left(\frac{\chi(3\sin^2\alpha - 2)}{\chi\cos^2\alpha + (\sin\alpha + \xi)^2 + \xi^2} + 2 - \sin^2\alpha\right)}{|D|} \tag{38}$$

and

$$\xi = r/L, \quad c_y = r\cot\alpha - h \tag{39}$$

$$|D| = 24\chi\sin^4\alpha + 12(\cos(2\alpha) + 3)\left((\sin\alpha + \xi)^2 + \xi^2\right) \tag{40}$$

Here, c_y is the nominal rotation center which is the intersection point of the limbs as shown in Fig. 10.

The compliance of the flexure platform mechanism is determined by six parameters $\mathbf{p}_{3ww} = (l/EI_z, \chi, \xi, \alpha, r, h)$.

5.2 Compliance Analysis and Synthesis. With regard to the analysis and synthesis of compliance, we can draw the following conclusions by observing compliance elements of $[C_{3ww}]$.

(1) All compliance elements are proportional to l/EI_z and $1/|D|$. This is the overall compliance of the platform in all directions. l/EI_z is the rotational compliance of a wire flexure. And the plot $1/|D|$ versus angle α, $\alpha \in$ [15 deg,75 deg] with Poisson's ratio $\nu = 0.3$ and $\xi = r/L \in [0,2]$ is shown in Fig. 11. To achieve a desired compliance, obviously one can chose appropriate values for width l, diameter d of the cross section as well as values of α, χ, ξ.

(2) Notice the second column and the fifth row are zero. This means that there is no translational compliance on the y axis. This is due to the simplification step (18). If we are interested in this parasitic error, we would have to use Eq. (17) instead. This is consistent with our intuition and our qualitative study [37].

(3) The instant rotation center for forces F_x and F_z can be obtained by computing

$$\frac{c_{41}}{c_{31}} = -\frac{c_{63}}{c_{13}} = c_y \tag{41}$$

This shows that when a lateral force F_x is applied, the motion of the stage is instantaneously equivalent to a rotation about the line through the instant rotation center parallel to z axis. Similarly, a force F_z will cause a rotation about the line through the center and parallel to x axis. Once again, this is consistent with our qualitative study.

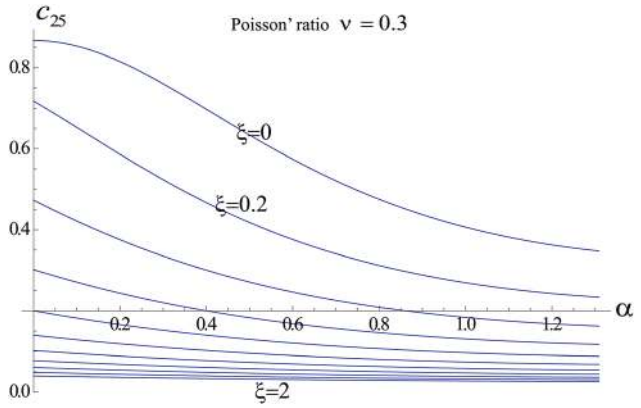

Fig. 12 The rotational compliance c_{25} versus $\alpha \in$ [15 deg,75 deg] with Poisson's ratio $\nu = 0.3$ and $\xi = r/L \in [0,2]$

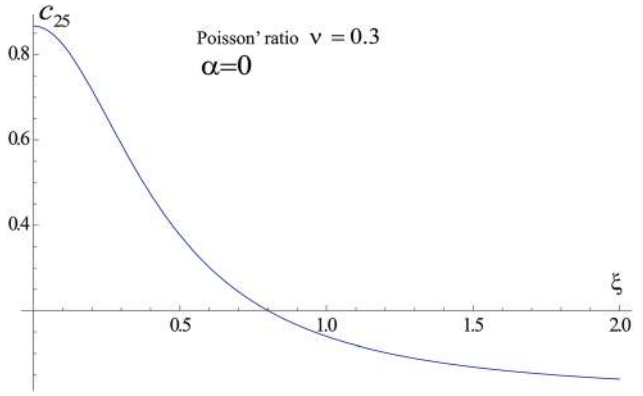

Fig. 13 The rotational compliance c_{25} versus $\xi = r/L \in [0,2]$ with Poisson's ratio $\nu = 0.3$ and $\alpha = 0$

(4) The translational compliance along x and z axes is the same due to the symmetry of the platform, calculated as

$$\frac{\delta_x}{F_x} = \frac{\delta_z}{F_z} = \frac{l}{EI_z} c_{41} = \frac{l}{EI_z} \frac{16 \sin \alpha^2 c_y^2}{|D|} \tag{42}$$

Obviously, one way to increase these two compliances is to increase the value of c_y which is determined by r,α,h as shown in Eq. (39).

(5) The rotational compliance along x and z axes is also the same, calculated as

$$\frac{\theta_x}{M_x} = \frac{\theta_z}{M_z} = \frac{l}{EI_z} c_{14} = \frac{l}{EI_z} \frac{16 \sin^2 \alpha}{|D|} \tag{43}$$

Obviously, the larger the angle α, the larger of these two compliances are. When $\alpha = 0$, we have a platform with three parallel limbs along the vertical line. One can easily see that this is consistent with our intuition that the rotational compliance about x and z axes will be zero for this case.

(6) The rotational compliance about y axis is the most complicated one. Let us plot the compliance element c_{25} versus α and ξ in Fig. 12. In general, this compliance drops as the assembly angle α and ξ increases.

(7) When $\alpha = 0$, we obtain a parallel platform with three vertical limbs. The compliance coefficient c_{25} becomes

$$c_{25} = \frac{1}{3(\chi + 2\xi^2)}$$

which is plotted in Fig. 13. As we can see, the compliance decreases drastically as $\xi = r/L$ increases.

5.3 Numerical Example. In this section, we use a numerical example to compare three compliance models: analytical model, simplified analytical model, and the finite element model. The dimensions of the flexure platform are $l = 20\,\text{mm}, L = 264\,\text{mm}$, $d = 1.3\,\text{mm}$, $r = 70/\sqrt{3}$, $h = 15\,\text{mm}$, $\alpha = 11.13$ deg, $E = 210$ GPa, $\nu = 0.3$

The analytical model is based on the wire flexure equation (17) without the assumption $l \ll L$. The simplified analytical model is based on the simplified wire flexure equation (18) which assumes $l \ll L$. And in the finite element model, we modeled the platform as a monolithic part which is meshed into 766,486 3D tetrahedral elements in ABAQUS. The base of the flexure mechanism is fixed. The load is applied to the center of the top piece and is limited within the range of linear deformation.

Table 1 Comparison of three compliance models

Compliance element	Analytical (original)	Analytical (simplified)	FE
δ_x/F_x[a]	2.07×10^{0}	$2.17 \times 10^{+0}$	$2.03 \times 10^{+0}$
θ_z/F_x	6.22×10^{-1}	6.53×10^{-1}	6.11×10^{-1}
δ_y/F_y	4.97×10^{-5}	4.97×10^{-5}	6.82×10^{-5}
θ_y/F_y	$0.00 \times 10^{+0}$	$0.00 \times 10^{+0}$	-1.16×10^{-5}
δ_z/F_z[a]	$2.07 \times 10^{+0}$	$2.17 \times 10^{+0}$	$2.03 \times 10^{+0}$
θ_x/F_z	-6.22×10^{-1}	-6.53×10^{-1}	-6.11×10^{-1}
δ_z/M_x	-1.09×10^{-2}	-1.14×10^{-2}	-1.07×10^{-2}
θ_x/M_x	3.27×10^{-3}	3.44×10^{-3}	3.21×10^{-3}
δ_y/M_y	$0.00 \times 10^{+0}$	$0.00 \times 10^{+0}$	-2.04×10^{-7}
θ_y/M_y[a]	2.49×10^{-2}	2.53×10^{-2}	2.41×10^{-2}
δ_x/M_z	1.09×10^{-2}	1.14×10^{-2}	1.07×10^{-2}
θ_z/M_z	3.27×10^{-3}	3.44×10^{-3}	3.21×10^{-3}

[a]Major compliance elements. Elements not listed are zeros. Units: $F_{x,y,z}$ (N), $M_{x,y,z}$ (N mm), $\delta_{x,y,z}$ (mm), and $\theta_{x,y,z}$ (deg).

The results are tabulated in Table 1, where the unit for force component is Newton, and the units for translational and rotational displacements are millimeter and degrees, respectively. We can draw the following conclusions.

(1) The horizontal compliance $\delta_x/F_x = \delta_z/F_z = 2.07 \times 10^{+0}$ is significantly larger than the vertical compliance $\delta_y/F_y = 4.97 \times 10^{-5}$. This all well agrees with our intuition and as well as the qualitative study by Su [37].

(2) The rotational compliance about the vertical axis θ_y/M_y is about 7.5 times larger than θ_x/M_x and θ_z/M_z. By observing the plot in Fig. 12, it is not hard to see that we can increase the relative rotational compliance about y axis over the compliance about x and z axes by decreasing the assembly angle α and/or increasing the ratio ξ. However, this goal is not achievable by changing l/EI_z, the compliance of the wire flexures, as shown in Sec. 5.2 of conclusion 1.

(3) The results of the analytical model are very close to the FE model for three major compliances δ_x/F_x, δ_z/F_z, and θ_y/M_y. The maximum error is less than 2%.

(4) The errors of the simplified analytical model are less than 7% compared with the FE model. This is due to the fact that we omitted l in Eq. (17) since we assume $l \ll L$.

6 Conclusion

A symbolic formulation for characterizing the compliance of general flexure mechanisms is presented. We categorize flexure mechanisms into serial chains, parallel chains, or hybrid structures. We first derive the symbolic formulation of the compliance

and stiffness matrices for a list of commonly used flexure elements. Based on these formulations, we derived the compliance matrices for more complicated flexure joints and simple chains. We aim to build a comprehensive library of compliance matrices for commonly used flexure structures. To analyze the compliance of a general flexure mechanism, we first divide the mechanism into building blocks or modules, analyze each module locally, and then build the compliance matrix from bottom-up. These symbolic formulas are beneficial to designers in that their geometric interpretation is more intuitive, they are computationally more efficient and greatly simplify more demanding tasks, such as design synthesis/optimization and sensitivity analysis. This design framework will be a systematical and robust tool for the analysis and design of general 3D flexure mechanisms.

Acknowledgment

The first two authors acknowledge funding provided by the National Science Foundation grant for this research.

Nomenclature

E = Young's modulus
G = shear modulus
χ = G/E, ratio of shear modulus and Young's modulus
ν = Poisson's ratio
$\mathbf{P}$ = geometric parameters of flexures
A = area of a cross section
I_y = area moment of inertia about y axis
I_z = area moment of inertia about z axis
J = polar moment of inertia
$\beta = J/I_z$
$\hat{T}$ = instantaneous motion twist representing deformation
$\hat{W}$ = a wrench representing the loading exerted
$[Ad]$ = a 6×6 adjoint transformation matrix
$[R]$ = a 3×3 rotational matrix
$[C]$ = a 6×6 compliance matrix
$[K]$ = a 6×6 stiffness matrix
$F_{x,y,z}$ = external force applied along x,y, or z axis
$M_{x,y,z}$ = external moment applied about x,y, or z axis
$\delta_{x,y,z}$ = translational deformation along x,y, or z axis
$\theta_{x,y,z}$ = rotational deformation about about x,y, or z axis

References

[1] Smith, S. T., 2000, *Flexure: Element of Elastic Mechanisms*, CRC Press LLC, London, United Kingdom.
[2] Smith, S. T., and Chetwynd, D. G., 1992, Foundations of Ultra-Precision Mechanism Design, CRC Press LLC, London, UK.
[3] Culpepper, M. L., and Anderson, G., 2004, "Design of a Low-Cost Nano-Manipulator Which Utilizes a Monolithic, Spatial Compliant Mechanism," Precis. Eng., **28**(4), pp. 469–482.
[4] Dagalakis, N. G., and Amatucci, E., 2001, "Kinematic Modeling of a 6 Degree of Freedom Tri-Stage Micro-Positioner," *Proceedings of the American Society for Precision Engineering 16th Annual Meeting*, Crystal City, VA, Nov. 10–15, pp. 200–203.
[5] Aguirre, A. D., Hertz, P. R., Chen, Y., Fujimoto, J. G., Piyawattanametha, W., Fan, L., and Wu, M. C., 2007, "Two-Axis MEMS Scanning Catheter for Ultra-high Resolution Three-Dimensional and En Face Imaging," Opt. Express, **15**(5), pp. 2445–2453.
[6] Henein, S., Frommherz, U., Betemps, R., Kalt, H., Ellenberger, U., Flechsig, U., and Raabe, J., 2007, "Mechanical Design of a Spherical Grating Monochromator for the Microspectroscopy Beamline Pollux at the Swiss Light Source," AIP Conf. Proc., **879**(1), pp. 643–646.
[7] Dimentberg, F., 1965, "The Screw Calculus and Its Applications in Mechanics," Foreign Technology Division, Wright-Patterson Air Force Base, OH, Technical Report No. FTD-HT-23–1632-67.
[8] Ball, R. S., 1998, *The Theory of Screws*, Cambridge University Press, Cambridge, England (Originally published in 1876 and revised by the author in 1900, now reprinted with an introduction by H. Lipkin and J. Duffy).
[9] Loncaric, J., 1987, "Normal Forms of Stiffness and Compliance Matrices," IEEE J. Rob. Autom., **3**(6), pp. 567–572.
[10] Lipkin, H., and Patterson, T., 1992, "Geometric Properties of Modelled Robot Elasticity: Part I—Decomposition," *Proceedings of ASME Design Technical Conferences*, DE-Vol. 45, pp. 187–193.
[11] Lipkin, H., and Patterson, T., 1992, "Geometric Properties of Modelled Robot Elasticity: Part II—Decomposition," *Proceedings of ASME Design Technical Conferences*, DE-Vol. 45, pp. 179–185.
[12] Patterson, T., and Lipkin, H., 1993, "Structure of Robot Compliance," ASME J. Mech. Des., **115**(3), pp. 576–580.
[13] Selig, J., and Ding, X., 2001, "A Screw Theory of Static Beams," *Proceedings of the 2001 IEEE/RSJ International Conference on Intelligent Robots and Systems*, Vol. 1, pp. 312–317.
[14] Selig, J. M., and Ding, X., 2009, "A Screw Theory of Timoshenko Beams," ASME J. Appl. Mech., **76**(3), 031003.
[15] Hunt, K. H., 1978, *Kinematic Geometry of Mechanisms*, Oxford University Press, New York.
[16] Lipkin, H., and Duffy, J., 1985, "The Elliptic Polarity of Screws," ASME J. Mech., Transm., Autom. Des., **107**(3), pp. 377–386.
[17] Mises, R. V., 1924, "Motorrechnung, ein neues hilfsmittel der mechanik," ZAMM—J. Appl. Math. Mech.(*Zeitschrift fr Angewandte Mathematik und Mechanik*), **4**(2), pp. 155–181. (English Translation by Baker, E. J., and Wohlhart, K., 1996, *Motor Calculus, A New Theoretical Device for Mechanics*, Institute for Mechanics, University of Technology Graz, Austria).
[18] Awtar, S., Slocum, A. H., and Sevincer, E., 2007, "Characteristics of Beam-Based Flexure Modules," ASME J. Mech. Des., **129**(6), pp. 625–639.
[19] Dai, J. S., and Ding, X., 2006, "Compliance Analysis of a Three-Legged Rigidly-Connected Platform Device," ASME J. Mech. Des., **128**(4), pp. 755–764.
[20] Patil, C. B., Sreenivasan, S. V., and Longoria, R. G., 2008, "Analytical and Experimental Characterization of Parasitic Motion in Flexure-Based Selectively Compliant Precision Mechanisms," *Proceedings of the ASME IDETC/CIE*, pp. 393–404.
[21] Pei, X., Yu, J., Zong, G., Bi, S., and Su, H., 2009, "The Modeling of Cartwheel Flexural Hinges," Mech. Mach. Theory, **44**(10), pp. 1900–1909.
[22] Awtar, S., and Sen, S., 2010, "A Generalized Constraint Model for Two-Dimensional Beam Flexures: Nonlinear Load-Displacement Formulation," ASME J. Mech. Des., **132**(8), p. 081008.
[23] Awtar, S., and Sen, S., 2010, "A Generalized Constraint Model for Two-Dimensional Beam Flexures: Nonlinear Strain Energy Formulation," ASME J. Mech. Des., **132**(8), p. 081009.
[24] Her, I., and Midha, A., 1987, "A Compliance Number Concept for Compliant Mechanisms, and Type Synthesis," ASME J. Mech., Transm., Autom. Des., **109**(3), pp. 348–355.
[25] Midha, A., Murphy, M. D., and Howell, L. L., 1997, "Compliant Constant-Force Mechanism and Devices Formed Therewith," U.S. Patent and Trademark Office, Washington, DC, U.S. Patent No. 5,649,454.:
[26] Huang, S., and Schimmels, J. M., 1998, "The Bounds and Realization of Spatial Stiffnesses Archieved With Simple Springs Connected in Parallel," IEEE Trans. Rob. Autom., **14**(3), pp. 466–475.
[27] Huang, S., and Schimmels, J. M., 2000, "The Bounds and Realization of Spatial Compliance Archieved With Simple Serial Elastic Mechanisms," IEEE Trans. Rob. Autom., **16**(1), pp. 99–103.
[28] Kim, C. J., Kota, S., and Moon, Y.-M., 2006, "An Instant Center Approach Toward the Conceptual Design of Compliant Mechanisms," ASME J. Mech. Des., **128**(3), pp. 542–550.
[29] Krishnan, G., Kim, C., and Kota, S., 2011, "An Intrinsic Geometric Framework for the Building Block Synthesis of Single Point Compliant Mechanisms," ASME J. Mech. Rob., **3**(1), p. 011001.
[30] Krishnan, G., Kim, C., and Kota, S., 2009, "Design Synthesis of 2-d Compliant Mechanisms Utilizing Serial Concatenation of Building Blocks," *ASME Conference Proceedings*, pp. 299–312.
[31] Hartmann, F., and Katz, C., 2007, *Structural Analysis With Finite Elements*, 2nd ed., Springer, New York.
[32] Kassimali, A., 2011, *Matrix Analysis of Structures*, 2nd ed., CL-Engineering, Stamford, CT.
[33] Petri, P. A., 2002, "A Continuum Mechanic Design Aid for Non-Planar Compliant Mechanisms," Master's thesis, MIT, Cambridge, MA.
[34] Selig, J., 1996, *Geometrical Methods in Robotics*, Springer Verlag, New York.
[35] McCarthy, J. M., 2000, *Geometric Design of Linkages*, Springer-Verlag, New York.
[36] Young, W. C., and Budynas, R. G., 2001, *Roark's Formulas for Stress and Strain*, 7th ed., McGraw-Hill, New York.
[37] Su, H.-J., 2011, "Mobility Analysis of Flexure Mechanisms Via Screw Algebra," ASME J. Mech. Rob., **3**(4), p. 041010.
[38] Blanding, D. L., 1999, *Exact Constraint: Machine Design Using Kinematic Processing*, ASME Press, New York.
[39] Zhang, S., and Fasse, E. D., 2001, "A Finite-Element-Based Method to Determine the Spatial Stiffness Properties of a Notch Hinge," ASME J. Mech. Des., **123**(1), pp. 141–147.
[40] Lobontiu, N., 2003, *Compliant Mechanisms: Design of Flexure Hinges*, CRC Press, London, UK.
[41] Yong, Y. K., Lu, T.-F., and Handley, D. C., 2008, "Review of Circular Flexure Hinge Design Equations and Derivation of Empirical Formulations," Precis. Eng., **32**(2), pp. 63–70.
[42] Ding, X., and Selig, J. M., 2004, "On the Compliance of Coiled Springs," Int. J. Mech. Sci., **46**(5), pp. 703–727.
[43] Zhang, S., 1999, "Lumped-Parameter Modelling of Elastically Coupled Bodies: Derivation of Constitutive Equations and Determination of Stiffness Matrices," Ph.D. thesis, The University of Arizona, Tucson, AZ
[44] Fasse, E. D., and Breedveld, P. C., 1998, "Modeling of Elastically Coupled Bodies: Part II—Exponential and Generalized Coordinate Methods," ASME J. Dyn. Syst., Meas., Control, **120**(4), pp. 501–506.